Journal of Magnetic Resonance **145,** 216–229 (2000)
doi:10.1006/jmre.2000.2114, available online at http://www.idealibrary.com on IDEAL®

Calculation of Cross-Polarization Spectra Influenced by Slow Molecular Tumbling

Christian Mayer

Institut für Physikalische und Theoretische Chemie, Universität Duisburg, 47048 Duisburg, Germany

Received October 5, 1999; revised April 4, 2000

A numeric algorithm which is suitable for calculating lineshapes of cross-polarization spectra influenced by isotropic and anisotropic tumbling is proposed. It is based on a description of the cross-polarization process using single-transition operators combined with rotational diffusion represented by a stationary Markov operator. A corresponding Fortran program can be implemented on a regular personal computer. The calculations yield spectral lineshapes for various mixing times under given cross-polarization conditions which reflect the characteristics of molecular motion. Representative results show typical transient oscillations on powder spectra, the dependence of the lineshapes on the degree of mobility, the effects of sample spinning, the consequence of a given deviation from the Hartmann–Hahn condition, and the effect of additional dipolar coupling between I spins. The applicability of the algorithm is demonstrated on supercooled glycerol as a model system.

Key Words: **cross polarization; motion; lineshape; simulation; algorithm.**

INTRODUCTION

Cross polarization between rare and abundant nuclei has developed into a powerful tool in the field of solid-state NMR, especially when it comes to the observation of ^{13}C nuclei in their natural abundance in the presence of protons (*1, 2*). A crucial step for the polarization transfer between two types of nuclei is a period of thermal contact ("mixing") between the two spin ensembles for which, in case of the common solid-state variety, the Hartmann–Hahn condition $\gamma_I H_{1I} = \gamma_S H_{1S}$ must be fulfilled (*1*). Experimentally, this is easy to accomplish in the case of static molecules with corresponding wide lines in the frequency spectrum. Rapid molecular reorientation inhibits the magnetization transfer as it leads to motional averaging of the dipolar coupling interaction.

An interesting situation is represented by the case of slow motion with correlation times similar to the time scale of cross polarization. Under this condition, the process of molecular reorientation will directly interact with the transfer of magnetization, leading to a cross-polarization pattern reflecting the characteristic parameters of the motion. Of course, the resulting lineshape is further influenced by partial motional averaging during the following free induction decay. The situation becomes even more complicated when sample spinning is introduced, e.g., in a magic angle spinning (MAS) experiment (*3*), or when adiabatic passage through the Hartmann–Hahn condition is applied (*4, 5*). In addition, the characteristic oscillations of the signal amplitude with increasing mixing time are strongly affected by molecular motion.

In all these cases, for a detailed analysis of the experimental results, it is necessary to find methods to simulate cross-polarization processes based on given motional and experimental parameters. Various analytical approaches have been proposed for the calculation of the magnetization transfer under some of the described conditions (*6–9*). They yield cross-relaxation rates T_{IS}^{-1} depending on molecular orientation, motional correlation times, or MAS parameters.

In the following, a numeric algorithm for isolated pairs of coupled spins (e.g., ^{13}C–^{1}H) is proposed which allows one to include all these effects simultaneously in order to simulate the development of lateral magnetization. It is based on the definition of discrete orientations (sites) which are considered to exchange certain quantities of magnetization per time unit depending on the type and rate of the motion. In addition, discrete steps in time which in some respect correspond to the dwell time of the experiment are introduced (*10*). This approximation accounts for the effect of molecular reorientations within a wide range of correlation times. Generally, the only preconditions are motional time constants that are at least three orders of magnitude larger than the reciprocal Larmor frequency. However, the finite element approach works best if correlation times do not differ from the reciprocal anisotropy of the local interaction tensor by more than three orders of magnitude.

During the mixing period, cross correlation is described based on single-transition operators (*11*). The cross-polarization process for each site is treated individually, being visualized as the rotation of the difference magnetization vector in a given single-transition subspace. In the case of adiabatic passage through the Hartmann–Hahn condition or sample spinning, the rotation axes and frequencies for each site are time dependent.

Outside of the cross-polarization sequence, the effect of the

1090-7807/00 $35.00

local magnetic field is represented by a corresponding precession of site-specific magnetization vectors in the x'–y' plane of the rotating frame (*10*). The effect of π pulses is accounted for by appropriate vector rotations. The effect of magic angle spinning is introduced by a resulting time dependence of the local magnetic field (*12*).

Model calculations and a practical example are presented to demonstrate the power and the versatility of the described algorithm.

THEORETICAL CONSIDERATIONS

Cross Polarization: Description in a Single-Transition Operator Basis

For a system of two coupled spins I and S simultaneously irradiated by corresponding RF fields, the effective Hamiltonian in the doubly rotating frame is given by (*11, 13*)

$$\mathbf{H}_{\text{eff}} = \hbar(\Delta_I I_Z + \Delta_S S_Z + 2\pi D_{IS} I_Z S_Z + \omega_{1I} I_X + \omega_{1S} S_X) \quad [1]$$

with the resonance offset frequencies Δ_I and Δ_S, the precession frequencies ω_{1I} and ω_{1S} corresponding to the RF field strengths for I and S nuclei, and the dipolar coupling constant D_{IS} (in Hz). If this Hamiltonian is transformed into a tilted doubly rotating frame, where the z axes point along the effective fields (*11*)

$$\omega_{I,\text{eff}} = (\Delta_I^2 + \omega_{1I}^2)^{1/2} \quad [2a]$$

and

$$\omega_{S,\text{eff}} = (\Delta_S^2 + \omega_{1S}^2)^{1/2} \quad [2b]$$

it becomes

$$\begin{aligned}\mathbf{H}_{\text{eff}}/\hbar &= \omega_{I,\text{eff}} I_Z + \omega_{S,\text{eff}} S_Z + \frac{\Delta_I}{\omega_{I,\text{eff}}}\frac{\Delta_S}{\omega_{S,\text{eff}}} 2\pi D_{IS} I_Z S_Z \\ &\quad + \frac{1}{4}\frac{\omega_{1I}}{\omega_{I,\text{eff}}}\frac{\omega_{1S}}{\omega_{S,\text{eff}}} 2\pi D_{IS}[I^+S^- + I^-S^+] \quad [3a] \\ &= \omega_{I,\text{eff}} I_Z + \omega_{S,\text{eff}} S_Z + \cos\vartheta_I \cos\vartheta_S 2\pi D_{IS} I_Z S_Z \\ &\quad + \frac{1}{4}\sin\vartheta_I \sin\vartheta_S 2\pi D_{IS}[I^+S^- + I^-S^+], \quad [3b]\end{aligned}$$

with

$$\tan\vartheta_I = \frac{\omega_{1I}}{\Delta_I} \quad \text{and} \quad \tan\vartheta_S = \frac{\omega_{1S}}{\Delta_S}.$$

All nonsecular terms of the dipolar coupling have been omitted. If we assume that all I spins are irradiated exactly on resonance, we may further neglect the term containing $I_Z S_Z$ in Eqs. [3a] and [3b], since Δ_I becomes zero.

A very elegant approach for the following description of the cross-polarization process has been proposed by Ernst *et al.* (*11*). Here, the magnetization transfer is represented in a space spanned by four orthogonal single-transition operators:

$$I_Z^{(1,4)} = \tfrac{1}{2}(I_Z + S_Z) \quad [4a]$$

$$I_Z^{(2,3)} = \tfrac{1}{2}(I_Z - S_Z) \quad [4b]$$

$$I_X^{(2,3)} = \tfrac{1}{2}(I^+S^- + I^-S^+) \quad [4c]$$

$$I_Y^{(2,3)} = -i/2(I^+S^- - I^-S^+). \quad [4d]$$

Within this basis, the corresponding evolution of the magnetization of I and S spins can be described using the vector model. It is visualized as the rotation of the difference magnetization vector (Fig. 1) in the three-dimensional subspace of the (*2, 3*) transition while the component $I_Z^{(1,4)}$ remains constant (*11*). In this subspace, the dipolar coupling between the nuclei (now merely represented by the term containing $[I^+S^- + I^-S^+]$ in Eqs. [3a] and [3b]) is equivalent to a field along the $I_X^{(2,3)}$ axis with a corresponding precession frequency

$$\omega_X = \frac{1}{2}\frac{\omega_{1I}}{\omega_{I,\text{eff}}}\frac{\omega_{1S}}{\omega_{S,\text{eff}}} 2\pi D_{IS}. \quad [5]$$

In addition, any difference between $\omega_{I,\text{eff}}$ and $\omega_{S,\text{eff}}$ corresponds to a field along the $I_Z^{(2,3)}$ axis (represented by the term $[\omega_{I,\text{eff}} I_Z + \omega_{S,\text{eff}} S_Z]$ in Eqs. [3a] and [3b]) with a precession frequency

$$\omega_Z = \omega_{I,\text{eff}} - \omega_{S,\text{eff}}. \quad [6]$$

Both influences act simultaneously during the complete period of double irradiation. They may be replaced by a single effective field along an axis with a precession frequency ω and a tilt angle φ (Fig. 1) given by (*11*)

$$\omega = (\omega_X^2 + \omega_Z^2)^{1/2} \quad [7a]$$

$$\sin\varphi = \frac{\omega_X}{\omega} \quad [7b]$$

$$\cos\varphi = \frac{\omega_Z}{\omega} \quad [7c]$$

$$\tan\varphi = \frac{\omega_X}{\omega_Z}. \quad [7d]$$

The resulting time dependence of the coefficients c_X, c_Y, and c_Z of the difference magnetization vector (Fig. 1) can be derived by Euler transformations as

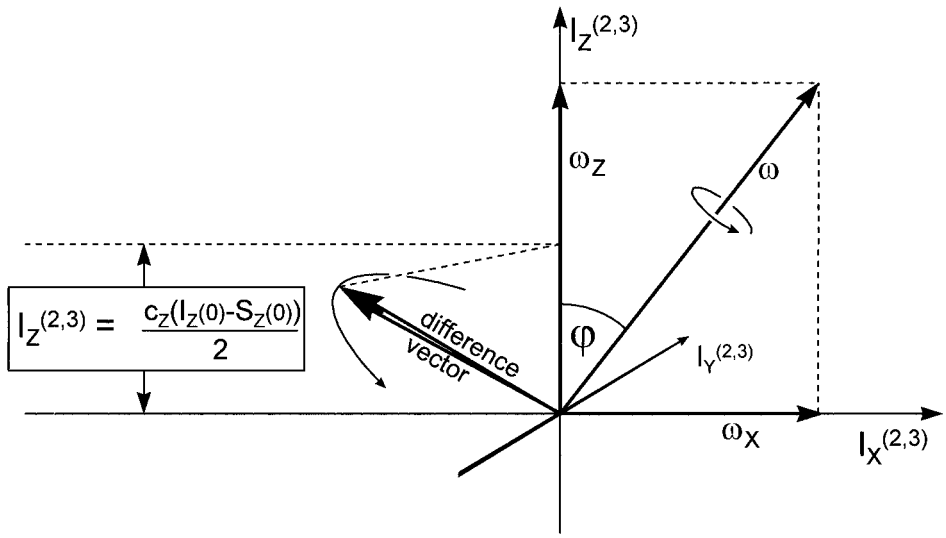

FIG. 1. Graphic representation of a cross-polarization process in an isolated I–S spin system as described in Ref. (*11*). The three axes describe a three-dimensional subspace $I_X^{(2,3)}$, $I_Y^{(2,3)}$, $I_Z^{(2,3)}$, within a system of four orthogonal single-transition operators $I_X^{(2,3)}$, $I_Y^{(2,3)}$, $I_Z^{(2,3)}$, and $I_Z^{(1,4)}$. Within this subspace, the difference magnetization vector evolves according to fields along the $I_X^{(2,3)}$ and the $I_Z^{(2,3)}$ axis which correspond to the dipolar interaction and the difference between effective frequencies, respectively. The $I_Z^{(2,3)}$ component of the difference vector (indicated by the level of the dotted lines on the left) is directly related to the amount of magnetization actually transferred between the spins I and S. The starting condition (zero polarization of S spins) is given by $c_Z = 1$, whereas complete magnetization transfer would correspond to $c_Z = -1$ (see text for details).

$$c'_X = \cos\varphi[(c_X\cos\varphi - c_Z\sin\varphi)\cos\omega t + c_Y\sin\omega t] + \sin\varphi[c_X\sin\varphi + c_Z\cos\varphi] \quad [8a]$$

$$c'_Y = -(c_X\cos\varphi - c_Z\sin\varphi)\sin\omega t + c_Y\cos\omega t \quad [8b]$$

$$c'_Z = -\sin\varphi[(c_X\cos\varphi - c_Z\sin\varphi)\cos\omega t + c_Y\sin\omega t] + \cos\varphi[c_X\sin\varphi + c_Z\cos\varphi], \quad [8c]$$

with c_X, c_Y, and c_Z being the coefficients before and c'_X, c'_Y, and c'_Z being those after the rotation. The observable magnetization for the S spins is obtained by subtracting the Z component of the difference magnetization vector from the constant term $\frac{1}{2}(I_Z(0) + S_Z(0))$ (see Fig. 1, left):

$$S_Z = \tfrac{1}{2}(I_Z + S_Z) - \tfrac{1}{2}(I_Z - S_Z) = \tfrac{1}{2}(I_Z(0) + S_Z(0)) - c_Z \cdot \tfrac{1}{2}(I_Z(0) - S_Z(0)). \quad [9]$$

Obviously, it is the ω_X pulse (Fig. 1) which leads to a periodic change of the coefficient c_Z (with $-1 \le c_Z \le 1$) equivalent to an oscillatory transfer of magnetization between I and S spins according to Eq. [9]. The efficiency of the transfer depends on the fulfillment of the Hartmann–Hahn condition, the coupling constant, the RF field strengths, and the resonance offsets. Complete transfer is obtained for $\omega_Z = 0$ and $\omega_X t = \pi$.

In most cases, the I–S spin system does not remain isolated, but comes in contact with a large number of additional I spins via I–I dipolar coupling. This necessarily gives rise to a broadening of the energy levels which determine the behavior of the I–S system (*14*). As the rotation parameters of the difference magnetization vector (Fig. 1) now differs for the various coupling situations, the overall vector decomposes into multiple components within the relevant coordinate system. Therefore, the resulting vector exhibits a characteristic decay which may be approximated by a monoexponential relaxation function with a characteristic time constant T_d. The observable linewidths of the I signals from a simple spectral lineshape experiment correspond directly to the contribution of the I–I dipolar coupling to the overall relaxation. These values may be determined experimentally on oriented samples, leading to a characteristic anisotropy of the time constant T_d. However, in most practical cases, these data are not known and the average time constant T_d for the relaxation of the difference vector has to be treated as a variable parameter to fit the observable damping of the oscillations. Equations [8a]–[8c] have to be modified accordingly to account for the exponential decay. Introducing the variables c''_X, c''_Y, and c''_Z as the new vector components after the rotation and the decay, we get

$$c''_X = c'_X\exp(-t/T_d) \quad [10a]$$

$$c''_Y = c'_Y\exp(-t/T_d) \quad [10b]$$

$$c''_Z = c'_Z\exp(-t/T_d). \quad [10c]$$

Consequently, the contact to other spins will lead to additional damping of the oscillations and finally to $c''_Z = 0$ equivalent to $I_Z(\infty) = S_Z(\infty) = \frac{1}{2}[I_Z(0) + S_Z(0)]$ (*11*). Here and in the following, all spin–lattice relaxation in the rotating frame will be ignored for simplicity.

This description of cross polarization is now integrated into an algorithm for numeric calculation of NMR experiments which has been proposed earlier (*10, 12*). Basically, the development of the difference vector is treated just as the development of the classical magnetization vector in the rotating frame. The basic idea of the algorithm and the practical method of implementation of the cp process will be described in the following.

Numeric Calculation of NMR Signals

For simulation of NMR results, we focus on the S spins and on the development of their magnetization in the x'–y' plane of the rotating frame (except for cp conditions, see below). In order to facilitate the numeric calculation, the Euler angles Φ, Θ, and Ψ, describing the orientation of the molecule with respect to the sample system, are segmented into $k_{\max}$, $l_{\max}$, and $m_{\max}$ discrete orientations leading to the definition of an overall number of $n_{\max} = k_{\max} \cdot l_{\max} \cdot m_{\max}$ sites (*12*). Within each site, the magnetization is represented by an independent and homogeneous ensemble of spins that can be treated classically. Even for very large site numbers, there are generally enough spins in each site to justify this approximation. The overall complex magnetization M (i.e., the signal observed in the x'–y' plane in the rotating frame) is then derived by simply adding all contributions $M(\Phi_k, \Theta_l, \Psi_m)$. In general, the contributions to the overall magnetization are time dependent and therefore given as $M(\Phi_k, \Theta_l, \Psi_m, t)$. In order to simplify the calculations, finite time steps Δt are introduced. The overall magnetization $M(t)$ consequently becomes

$$M(t) = M(n_t \cdot \Delta t) = \sum_{klm} M(\Phi_k, \Theta_l, \Psi_m, n_t \cdot \Delta t). \quad [11]$$

Of course, due to these approximations, it is crucial to choose the intervals in time and orientation small enough in order to avoid artifacts. For all calculations, it is absolutely necessary to check the results for convergence with increasing n and decreasing Δt. Common settings for these parameters vary between 10,000 and 500,000 steps in time (for situations close to the minimum of the spin–spin relaxation time and for situations near the limits of the dynamic range, respectively) as well as between 1000 and 1,000,000 angular orientations (for correlation times near the fast and slow limit of the dynamic range, respectively).

The starting value $M(\Phi_k, \Theta_l, \Psi_m, 0)$ for each site is given by the particular initial experimental condition, e.g., by the equilibrium populations P_{eq} (as after a $\pi/2$ pulse on a system in thermal equilibrium) or by zero (as typically for the beginning of cross polarization). In the following, the magnetization $M(\Phi_k, \Theta_l, \Psi_m, t)$ is affected by a variety of internal and external influences, such as

(a) interaction with local fields,
(b) molecular motion,
(c) π pulses,
(d) sample spinning, and
(e) cross polarization.

Some of these conditions are present throughout the experiment (typically a, b, and d), and some are limited to certain time intervals or act at specific points (as is assumed for c). Except for cross polarization (e), no interaction with other nuclei is taken into account, an assumption which represents complete heteronuclear decoupling. The effect of the influences a–e on the development of $M(t)$ in the numeric simulation will be discussed separately in the following sections.

(a) Interactions with local fields (chemical shift). Based on the stochastic Liouville equation, the magnetization vector for each site in the presence of an orientation-dependent Hamilton operator develops in the rotating frame according to

$$M(\Omega_n, t + \Delta t) = M(\Omega_n, t)\exp[i\omega(\Omega_n)\Delta t], \quad [12]$$

where Ω_n stands for a discrete orientation in space. The orientation-dependent frequencies $\omega(\Omega_n)$ are derived from the tensor of the local interaction, e.g., the chemical shift anisotropy (CSA) tensor $\mathbf{H}_{\text{CS}} = \gamma\hbar\mathbf{I}\sigma\mathbf{B}$, by a set of Euler transformations. Generally, the tensor elements are known in a magnetic tensor system (principal axis system), where all off-diagonal elements are zero:

$$\sigma^{\text{M}} = \begin{pmatrix} \sigma_{XX} & 0 & 0 \\ 0 & \sigma_{YY} & 0 \\ 0 & 0 & \sigma_{ZZ} \end{pmatrix}. \quad [13]$$

For the cases treated in the following text, this magnetic tensor system is chosen to be identical to the diffusion tensor system which is determined by the preferred rotation axes of the molecule (*12*). This simplification is possible for isotropic molecular motion. This given, the tensor in the laboratory system, which is defined by the orientation of the external magnetic field H_0, is obtained by a single transformation:

$$\sigma^{\text{L}} = \mathbf{T}^{\text{ML}}(\Phi_k, \Theta_l, \Psi_m)\sigma^{\text{M}}\mathbf{T}^{\text{ML}-1}(\Phi_k, \Theta_l, \Psi_m). \quad [14]$$

The corresponding set of Euler angles Φ_k, Θ_l, Ψ_m describes the common orientation Ω_n of molecules which belong to a

given site n. With the relation between the relevant tensor element σ^{S}_{ZZ} and the resonance frequency ω

$$\omega(\Omega_n) = \omega(\Phi_k, \Theta_l, \Psi_m) = \omega_0 \sigma^{S}_{ZZ}(\Phi_k, \Theta_l, \Psi_m) \quad [15]$$

the time evolution of the magnetization vector for each site may be calculated using Eq. [12].

(b) The effect of molecular motion. Generally, motion leads to an exchange of magnetization between the sites which are considered to remain fixed in space. For very short time intervals Δt, it is allowed to approximate the continuous exchange process by discontinuous steps (*10, 12*). This converts Eq. [12] into

$$\begin{aligned} M(\Omega_n, t + \Delta t) = {} & M(\Omega_n, t)\exp(i\omega(\Omega_n, t)\Delta t) \\ & + \sum_{n'} [-k_{(\Omega n \rightarrow \Omega n')}\Delta t M(\Omega_n, t)\exp(i\omega(\Omega_n, t)\Delta t) \\ & + k_{(\Omega n' \rightarrow \Omega n)}\Delta t M(\Omega_{n'}, t)\exp(i\omega(\Omega_{n'}, t)\Delta t)], \end{aligned} \quad [16]$$

where $k_{(\Omega n \rightarrow \Omega n')}$ stands for the first-order rate constant describing the transfer from the site Ω_n to site $\Omega_{n'}$. The rate constants depend on the velocity of the exchange induced by the individual reorientation process. For the example of anisotropic rotational diffusion, the motion is characterized by two correlation times $\tau_\parallel$ and $\tau_\perp$, referring to rotational diffusion along the long axis and the two short axes, respectively. Based on relative site populations P_{rel} defined as

$$P_{rel}(\Omega_n) = P(\Omega_n)/P_{eq}(\Omega_n) \quad [17a]$$

$$P_{eq}(\Omega_n) = \frac{\sin \Theta_l}{k_{max} m_{max} \sum_{l'} \sin \Theta_{l'}}, \quad [17b]$$

the corresponding diffusion operator can be formulated as (*15, 16*)

$$\Gamma_{dif} \mathbf{P}_{rel} = \frac{\partial P_{rel}}{\partial t} \quad [18]$$

$$\begin{aligned} \Gamma_{dif} = {} & \frac{1}{6\tau_\parallel} \frac{\partial^2}{\partial \Phi^2} + \frac{1}{6\tau_\perp} \left(\frac{\partial^2}{\partial \Theta^2} + \cot^2\Theta \frac{\partial^2}{\partial \Phi^2} + \frac{1}{\sin^2\Theta} \frac{\partial^2}{\Psi^2} \right. \\ & \left. - 2 \frac{\cot \Theta}{\sin \Theta} \frac{\partial^2}{\partial \Phi \partial \Psi} + \cot \Theta \frac{\partial}{\partial \Theta} \right). \end{aligned} \quad [19]$$

If this diffusion tensor is applied to the model of discrete orientations, it yields a set of first-order rate constants which describe the exchange processes between adjacent sites:

$$\begin{aligned} k(\Phi_k \rightarrow \Phi_{k+1}) &= k(\Phi_k \rightarrow \Phi_{k-1}) \\ &= \left(\frac{1}{6\tau_\parallel} + \frac{1}{6\tau_\perp} \cot^2\Theta \right) \frac{1}{(\Delta\Phi)^2} \end{aligned} \quad [20]$$

$$k(\Theta_l \rightarrow \Theta_{l\pm1}) = \frac{1}{6\tau_\perp} \frac{\sqrt{\sin \Theta_{l\pm1}}}{\sqrt{\sin \Theta_l}} \frac{1}{(\Delta\Theta)^2} \quad [21]$$

$$\begin{aligned} k(\Psi_m \rightarrow \Psi_{m+1}) &= k(\Psi_m \rightarrow \Psi_{m-1}) \\ &= \frac{1}{6\tau_\perp} \frac{1}{\sin^2\Theta} \frac{1}{(\Delta\Psi)^2} \end{aligned} \quad [22]$$

$$\begin{aligned} k\begin{pmatrix} \Phi_k \rightarrow \Phi_{k+1} \\ \Psi_m \rightarrow \Psi_{m+1} \end{pmatrix} &= k\begin{pmatrix} \Phi_k \rightarrow \Phi_{k-1} \\ \Psi_m \rightarrow \Psi_{m-1} \end{pmatrix} \\ &= -\frac{1}{6\tau_\perp} 2 \frac{\cot \Theta}{\sin \Theta} \frac{1}{4(\Delta\Phi)(\Delta\Psi)} \end{aligned} \quad [23]$$

$$\begin{aligned} k\begin{pmatrix} \Phi_k \rightarrow \Phi_{k+1} \\ \Psi_m \rightarrow \Psi_{m-1} \end{pmatrix} &= k\begin{pmatrix} \Phi_k \rightarrow \Phi_{k-1} \\ \Psi_m \rightarrow \Psi_{m+1} \end{pmatrix} \\ &= \frac{1}{6\tau_\perp} 2 \frac{\cot \Theta}{\sin \Theta} \frac{1}{4(\Delta\Phi)(\Delta\Psi)}. \end{aligned} \quad [24]$$

Integrated in Eq. [16], these rate constants simulate the effect of (an)isotropic rotational diffusion on $M(\Omega_n, t)$. In a similar manner, any other motional process may be described, which is especially straightforward in the case of jump motions. In the following, we will treat the case of isotropic rotational diffusion, where only one correlation time τ (with $\tau = \tau_\parallel = \tau_\perp$) is relevant.

(c) The effect of π pulses. So far, the algorithm describes the development of the magnetization of the S spins in the x'–y' plane. Therefore, and for simplicity, we restrict our discussion to π pulses and assume that their duration is infinitesimally short. If this is given, the magnetization right after a π pulse at $t = t_{pulse}$ may be derived from the magnetization just before the pulse according to

$$M(t_{pulse} + \Delta t) = [e^{-i\varphi} M(t_{pulse})]^* e^{i\varphi}, \quad [25]$$

where the asterisk denotes the conjugated complex and φ stands for the phase of the pulse (e.g., $\varphi = 0°$ for an x pulse). For an x pulse or a y pulse, the consequence is merely the inversion of the imaginary or the real part of the magnetization, respectively. For all other phases φ, $M(t_{pulse} + \Delta t)$ may be calculated according to Eq. [25].

(d) The effect of sample spinning. The additional motional process induced by sample spinning requires an additional set of Euler angles. In this case, the single transformation from the magnetic tensor system to the laboratory system as given in Eq. [14] has to be replaced by two transformations (*12*),

$$\sigma^{S} = \mathbf{T}^{MS}(\Phi_k, \Theta_l, \Psi_m)\sigma^{M}\mathbf{T}^{MS-1}(\Phi_k, \Theta_l, \Psi_m) \quad [26]$$

and

$$\sigma^{L} = \mathbf{T}^{SL}(\alpha, \beta, \gamma)\sigma^{S}\mathbf{T}^{SL-1}(\alpha, \beta, \gamma), \quad [27]$$

where the index S denotes a reference frame defined by the geometry of the sample container, e.g., the rotor in a sample spinning experiment. Due to the axial symmetry of the magnetic field, the result does not depend on the Euler angle γ, which therefore can be set to zero. The angle β describes the orientation of the sample rotation axis versus the magnetic field (e.g., 54.7° in the case of MAS), while α is time dependent with the frequency ω_r of the sample rotation according to

$$\alpha(t) = \omega_r t. \quad [28]$$

With the Euler transformations given above, the site- and time-dependent Larmor frequencies are derived from the relevant tensor element σ^{L}_{ZZ} in the laboratory frame according to (*12*)

$$\begin{aligned}\omega(\Omega_n, t) &= \omega_0\sigma^{L}_{ZZ}(\Phi_k, \Theta_l, \Psi_m, t)\\ &= \omega_0\{[\cos^2\beta\sigma^{S}_{ZZ}] + \sin^2(\omega_r t)[\sin^2\beta\sigma^{S}_{YY}]\\ &\quad + \cos^2(\omega_r t)[\sin^2\beta\sigma^{S}_{XX}] + \sin(\omega_r t)\cos(\omega_r t)\\ &\quad \times [\sin^2\beta(\sigma^{S}_{XY} + \sigma^{S}_{YX})] + \sin(\omega_r t)\\ &\quad \times [\sin\beta\cos\beta(\sigma^{S}_{YZ} + \sigma^{S}_{ZY})] + \cos(\omega_r t)\\ &\quad \times [\sin\beta\cos\beta(\sigma^{S}_{XZ} + \sigma^{S}_{ZX})]\} \quad [29]\end{aligned}$$

with the elements of σ^{S} given by Eq. [26]. Introduced into Eq. [12] for the static case or into Eq. [16] in the case of molecular motion, these site- and time-dependent Larmor frequencies account for the effect of sample rotation at any given rotation angle β and rotation frequency ω_r.

(e) The effect of cross polarization. In order to simulate the influence of the cp condition on the magnetization of the S spins, we consider I–S spin pairs with dipolar coupling given by a coupling constant D_{IS}. With this assumption, it is possible to introduce the description of the cp experiment outlined in the initial section. To begin with, the dipolar coupling constant has to be determined for every site Ω_n and, in the case of sample spinning, also for any given time t. The values for the dipolar coupling constants $D_{IS}(\Omega_n, t)$ in hertz as needed in Eq. [5] are given by

$$D_{IS}(\Omega_n, t) = \frac{1}{2\pi}\frac{\mu_0\gamma_I\gamma_S\hbar}{4\pi r^3_{IS}}(1 - 3\cos^2\theta_{IS}(\Omega_n, t)), \quad [30]$$

with r_{IS} being the internuclear distance between I and S and with $\theta_{IS}(\Omega_n, t)$ representing the angle between the vector $\mathbf{r}_{IS}$ and the magnetic field for each site Ω_n at a given time t.

Generally, an initial thermal equilibrium, a $\pi/2$ pulse on the I spins, and a subsequent mixing period will represent the starting condition of the cp experiment. Therefore, we assume that $M(\Omega_n, 0) = 0$ (which always refers to the S spins) for all sites. In the single-transition operator basis in the tilted doubly rotating frame with all protons exactly on resonance, the initial situation corresponds to a detectable magnetization given by

$$S_Z(\Omega_n, 0) = 0 \quad [31]$$

$$I_Z(\Omega_n, 0) = sP_{eq}(\Omega_n). \quad [32]$$

The scaling factor s may be chosen arbitrarily and is given the value of 2.0 in the following. The time-dependent observable magnetization of the S spins is then derived according to Eq. [9]:

$$\begin{aligned}S_Z(\Omega_n, t) &= \frac{I_Z(\Omega_n, 0) + S_Z(\Omega_n, 0)}{2}\\ &\quad - \frac{c_Z(\Omega_n, t)[I_Z(\Omega_n, 0) - S_Z(\Omega_n, 0)]}{2}\\ &= [1 - c_Z(\Omega_n, t)]\frac{I_Z(\Omega_n, 0)}{2}\\ &= [1 - c_Z(\Omega_n, t)]P_{eq}(\Omega_n). \quad [33]\end{aligned}$$

The coefficients c_Z may be replaced by weighted coefficients d_Z which account for the relative contribution of each site to the overall magnetization. With $d_Z = c_Z(\Omega_n, t)P_{eq}(\Omega_n)$ Eq. [33] becomes

$$S_Z(\Omega_n, t) = P_{eq}(\Omega_n) - d_Z(\Omega_n, t). \quad [34]$$

The development of the magnetization of the S spins for each site now is completely determined by the development of the corresponding coefficients $d_Z(\Omega_n, t)$. From Eqs. [31] and [34], it is obvious that the starting condition is given by

$$d_Z(\Omega_n, 0) = P_{eq}(\Omega_n) \quad [35]$$

for all sites. With Eqs. [8a]–[8c] and accounting for the decay of the difference magnetization vector according to Eqs. [10a]–[10c], the time dependence of the full set of coefficients in the given algorithm is represented by

$$d_x(\Omega_n, t + \Delta t) = d'_X(\Omega_n, t) \quad [36a]$$

$$d_y(\Omega_n, t + \Delta t) = d'_Y(\Omega_n, t) \quad [36b]$$

$$d_z(\Omega_n, t + \Delta t) = d'_Z(\Omega_n, t), \quad [36c]$$

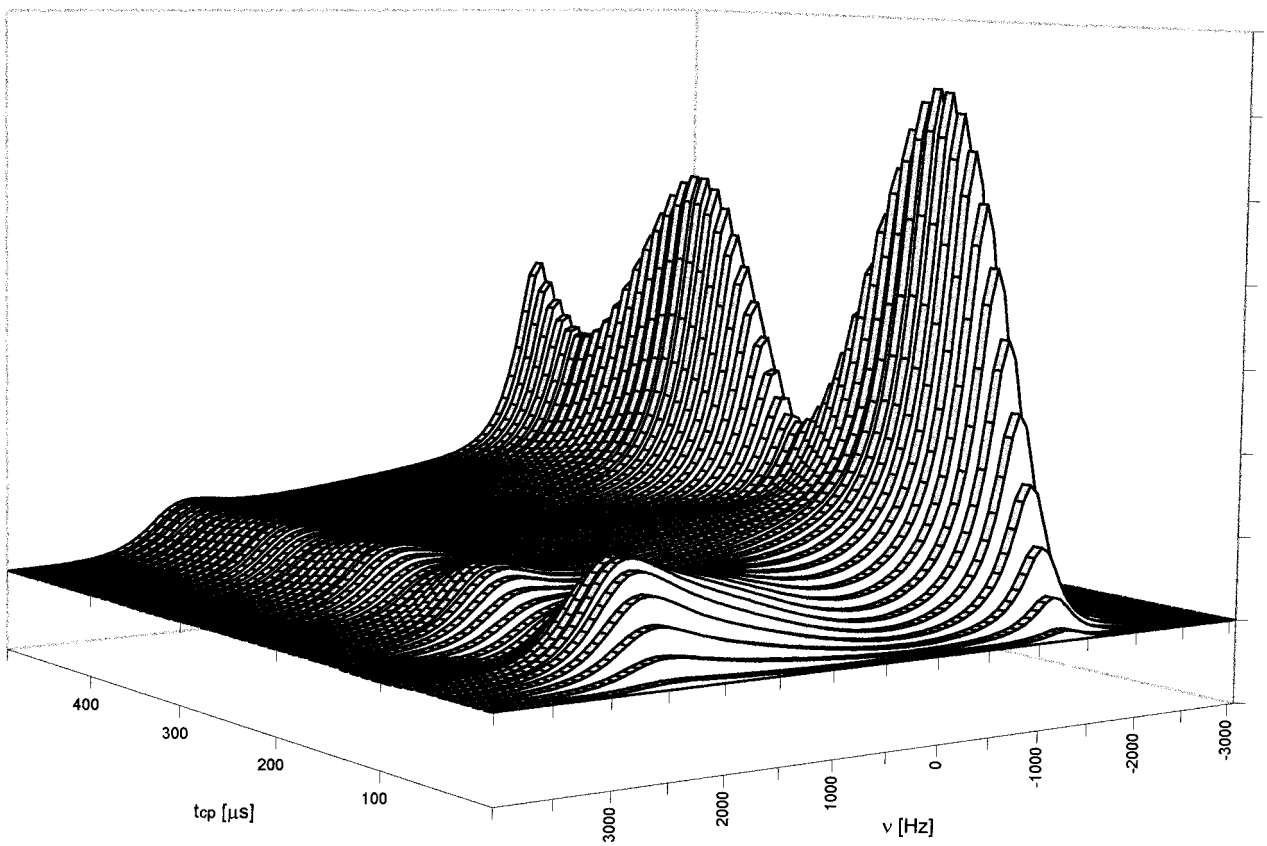

FIG. 2. Stacked plot of calculated spectral lineshapes obtained under variation of the cross-polarization mixing time t_{cp}. The values for t_{cp} vary between 10 μs (front) and 500 μs (back) in steps of 10 μs. The motional mechanism is represented by isotropic rotational diffusion with a correlation time of 1 ms. All other parameters for the simulated cross-polarization process are given in the text.

where

$$\begin{aligned} d'_X(\Omega_n, t) = \{&\cos\varphi[(d_X(\Omega_n, t)\cos\varphi \\ &- d_Z(\Omega_n, t)\sin\varphi)\cos(\omega\Delta t) \\ &+ d_Y(\Omega_n, t)\sin(\omega\Delta t)] \\ &+ \sin\varphi[d_X(\Omega_n, t)\sin\varphi \\ &+ d_Z(\Omega_n, t)\cos\varphi]\}\exp(-\Delta t/T_d) \end{aligned} \quad [37a]$$

$$\begin{aligned} d'_Y(\Omega_n, t) = \{&-(d_X(\Omega_n, t)\cos\varphi \\ &- d_Z(\Omega_n, t)\sin\varphi)\sin(\omega\Delta t) \\ &+ d_Y(\Omega_n, t)\cos(\omega\Delta t)\}\exp(-\Delta t/T_d) \end{aligned} \quad [37b]$$

$$\begin{aligned} d'_Z(\Omega_n, t) = \{&-\sin\varphi[(d_X(\Omega_n, t)\cos\varphi \\ &- d_Z(\Omega_n, t)\sin\varphi)\cos(\omega\Delta t) \\ &+ d_Y(\Omega_n, t)\sin(\omega\Delta t)] \\ &+ \cos\varphi[d_X(\Omega_n, t)\sin\varphi \\ &+ d_Z(\Omega_n, t)\cos\varphi]\}\exp(-\Delta t/T_d). \end{aligned} \quad [37c]$$

In the most general case, the angles φ and the precession frequencies ω depend on the site (due to local fields) as well as on time (e.g., due to sample spinning or variable pulse amplitude) and are calculated according to Eqs. [5]–[7]. If all protons are irradiated on resonance, the resonance offset Δ_I becomes zero and Eqs. [5]–[7] result in

$$\begin{aligned} \omega(\Omega_n, t) &= (\omega_X^2 + \omega_Z^2)^{1/2} \\ &= \left\{\left[\frac{\omega_{1S}}{\omega_{S,\mathrm{eff}}(\Omega_n, t)}\,\pi D_{IS}(\Omega_n, t)\right]^2 \right. \\ &\qquad \left. + [\omega_{1I} - \omega_{S,\mathrm{eff}}(\Omega_n, t)]^2\right\}^{1/2} \end{aligned} \quad [38a]$$

$$\begin{aligned} \sin\varphi(\Omega_n, t) &= \frac{\omega_X(\Omega_n, t)}{\omega(\Omega_n, t)} \\ &= \frac{\omega_{1S}}{\omega_{S,\mathrm{eff}}(\Omega_n, t)}\,\pi D_{IS}(\Omega_n, t)\,\frac{1}{\omega(\Omega_n, t)} \end{aligned} \quad [38b]$$

$$\begin{aligned} \cos\varphi(\Omega_n, t) &= \frac{\omega_Z(\Omega_n, t)}{\omega(\Omega_n, t)} \\ &= [\omega_{1I} - \omega_{S,\mathrm{eff}}(\Omega_n, t)]\,\frac{1}{\omega(\Omega_n, t)}. \end{aligned} \quad [38c]$$

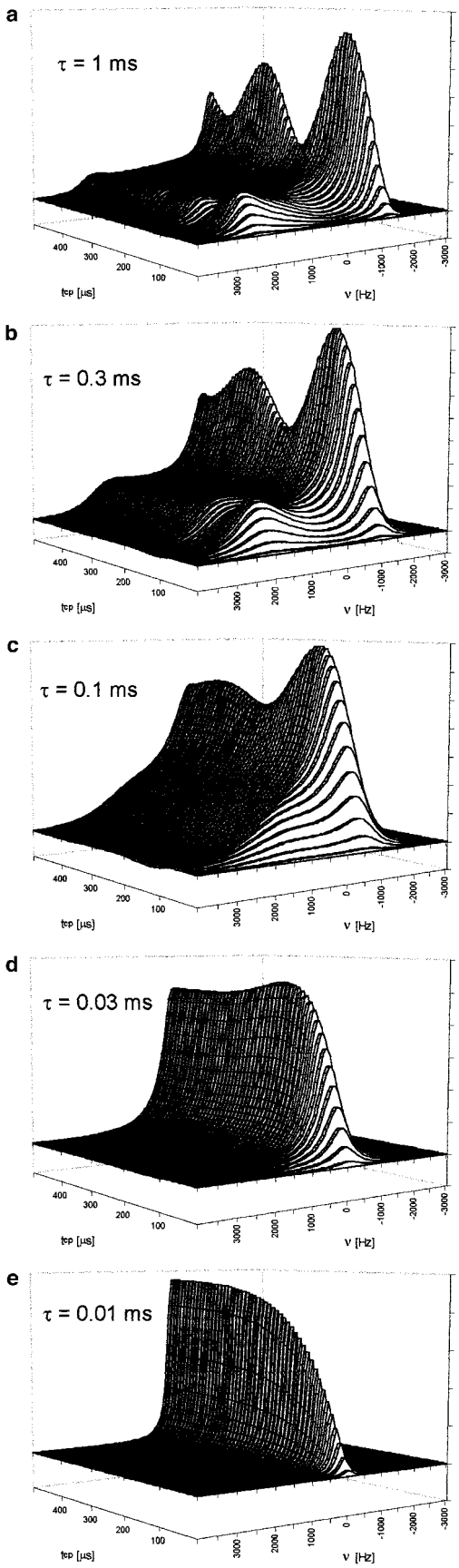

To account for adiabatic passage through the Hartmann–Hahn condition (e.g., by using ramped amplitude pulses) the spin lock frequency ω_{1S} may depend on time and therefore enter Eqs. [38a] and [38b] and Eq. [2b] as $\omega_{1S}(t)$.

In the presence of molecular motion, the exchange processes as described in part b lead to an additional time dependence of the coefficients. In this case, in analogy to Eq. [16], their time evolution is given by

$$d_X(\Omega_n, t + \Delta t) = d'_X(\Omega_n, t) + \sum_{n'} [-k_{(\Omega n \to \Omega n')} \Delta t d'_X(\Omega_n, t) + k_{(\Omega n' \to \Omega n)} \Delta t d'_X(\Omega_{n'}, t)] \quad [39a]$$

$$d_Y(\Omega_n, t + \Delta t) = d'_Y(\Omega_n, t) + \sum_{n'} [-k_{(\Omega n \to \Omega n')} \Delta t d'_Y(\Omega_n, t) + k_{(\Omega n' \to \Omega n)} \Delta t d'_Y(\Omega_{n'}, t)] \quad [39b]$$

$$d_Z(\Omega_n, t + \Delta t) = d'_Z(\Omega_n, t) + \sum_{n'} [-k_{(\Omega n \to \Omega n')} \Delta t d'_Z(\Omega_n, t) + k_{(\Omega n' \to \Omega n)} \Delta t d'_Z(\Omega_{n'}, t)]. \quad [39c]$$

In this manner, the coefficients are calculated step by step during the complete mixing period. At the end of this sequence, it is the coefficient d_z which yields the magnetization S_Z according to Eq. [34]. This set of magnetization elements $S_Z(\Omega_n, t)$ determines the starting condition $M(\Omega_n, t)$ for the following section of the experiment according to

$$M(\Omega_n, t) = \frac{\omega_{1S}}{\omega_{S,\mathrm{eff}}(\Omega_n, t)} S_Z(\Omega_n, t), \quad [40]$$

which accounts for the fact that the cross polarization is developing along the z axis of the tilted rotating frame which in most cases deviates from the x' axis of the classical rotating frame. All contributions $M(\Omega_n, t)$ are defined as real numbers as the signal is completely in phase after cross polarization. This phase is determined by the phase of the spin lock irradiation which is assumed to follow the x' axis of the rotating frame.

MODEL CALCULATIONS

All of the following representative results have been obtained considering a common cp experiment (initial mixing period t_{cp} followed by a free induction decay of the S spins) on a simple hypothetical two-spin system which is characterized by the following data:

FIG. 3. Stacked plots of calculated spectral lineshapes for various mixing times t_{cp} and various tumbling rates. The isotropic rotational diffusion is characterized by a single correlation time $\tau = \tau_\parallel = \tau_\perp$: (a) $\tau = 1$ ms, (b) $\tau = 0.3$ ms, (c) $\tau = 0.1$ ms, (d) $\tau = 0.03$ ms, and (e) $\tau = 0.01$ ms. All other simulation parameters are given in the text.

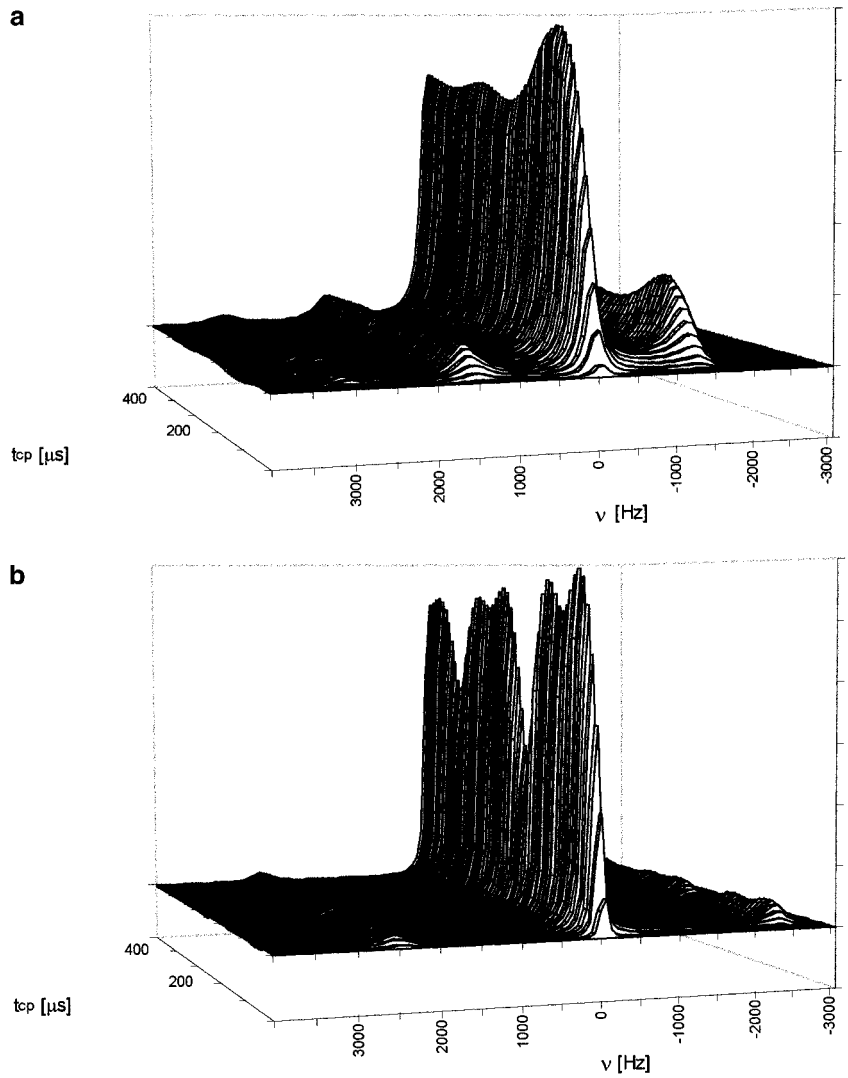

FIG. 4. Stacked plots of calculated spectral lineshapes for various mixing times t_{cp} under the influence of magic angle spinning at different rates of sample rotation ω_r: (a) $\omega_r/2\pi = 1.5$ kHz; (b) $\omega_r/2\pi = 2.5$ kHz. All other parameters are given in the text.

(a) The chemical shift tensor is axially symmetric with the tensor elements $\sigma_{XX} = -1500$ Hz, $\sigma_{YY} = -1500$ Hz, and $\sigma_{ZZ} = 3000$ Hz.

(b) The site- and time-dependent dipolar coupling is characterized by $D_{IS}(\Omega_n, t) = 10\text{ kHz} \cdot (1 - 3\cos^2\theta_{IS}(\Omega_n, t))$; the vector $\mathbf{r}_{IS}$ is considered to be parallel to the z axis of the magnetic tensor system.

(c) The spin lock frequencies ω_1 for both nuclei are set to 100,000 1/s, equivalent to a perfect Hartmann–Hahn match (except for the last example, where $\omega_{1,S}$ is 80,000 1/s; see below).

(d) The motional mechanism affecting the cp process and the resulting lineshapes is assumed to be an isotropic rotational diffusion.

(e) Except for the last example, the damping of the oscillations due to the I–I dipolar coupling has been neglected (T_d is set to infinity). In all these cases, damping is caused merely by molecular motions.

All these parameters represent rather basic and straightforward conditions. They are chosen deliberately in order to better visualize the expected phenomena. However, the described algorithm is versatile enough to account for any given chemical shift tensor, any orientation of the internuclear vector in the magnetic tensor system, any given deviation from the Hartmann–Hahn condition, and more complex motions such as anisotropic rotational diffusion or any jump process. In the following, spectral lineshapes are calculated under variation of the cross-polarization period t_{cp} and represented in stacked plots. The value for t_{cp} varies between 10 μs (front) and 500 μs

(back) in steps of 10 μs. As mentioned before, no spin–lattice relaxation is taken into account at this stage of the simulation. The number of angular orientations varies between 2000 and 5000; the development of the magnetization is simulated over 100,000 up to 200,000 time intervals. Under these conditions, the calculation of a full set of 50 spectra typically requires 3–15 h on a personal computer.

Transient Oscillations in a Powder Spectrum

The result of a lineshape calculation based on the data given above and a correlation time of 1 ms for the rotational diffusion is shown in Fig. 2. All single spectra represent powder patterns more or less distorted due to motion and incomplete polarization transfer. Especially for short mixing periods, they differ significantly from a corresponding lineshape obtained under simulation of direct excitation. The spectra show a characteristic amplitude oscillation with t_{cp} which, in the case of the 90° orientation of the axially symmetric tensor (near -1500 Hz spectral frequency), exhibits an oscillation frequency of approximately 5 kHz, and in the case of the 0° orientation (near 3000 Hz spectral frequency), exhibits an oscillation frequency of approximately 10 kHz, corresponding to the given dipolar coupling constant. In the vicinity of the magic angle (near 0 Hz spectral frequency), the oscillation frequency is zero. A similar dependence of the angular orientation is observed for the initial buildup of the cp spectrum, leading to a characteristic "hole" near the magic angle for $t_{cp} < 100$ μs. The observed oscillations correspond well with early experimental data on an oriented sample (*13*). In the simulation, they are merely damped by the effect of motional exchange. Under experimental conditions, this damping would be increased by further influences, e.g., by the interaction among I spins. A second Fourier transformation with respect to t_{cp} yields a two-dimensional spectrum with the chemical shift pattern along the first axis and the dipolar coupling pattern along the second axis (not shown).

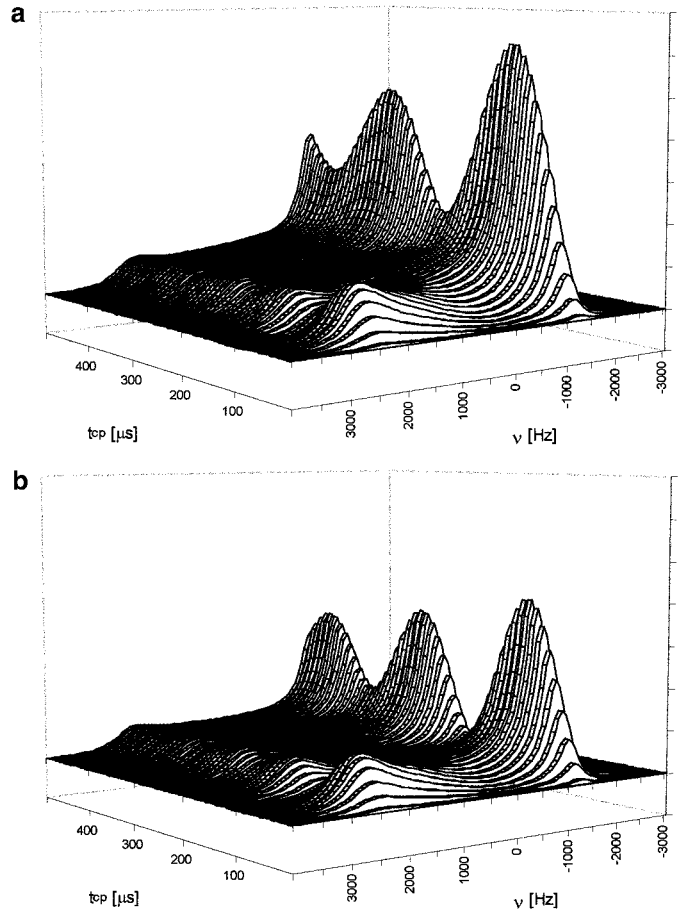

FIG. 5. Stacked plots of calculated spectral lineshapes for various mixing times t_{cp} influenced by isotropic rotational diffusion ($\tau = 1$ ms) with (a) ideal fulfillment of the Hartmann–Hahn condition and (b) deviation from the Hartmann–Hahn condition according to $\omega_{1I} = 100{,}000$ 1/s and $\omega_{1S} = 80{,}000$ 1/s. All other parameters are given in the text. The intensity axes of both plots a and b are of identical scale to allow direct comparison of spectral amplitudes.

Variation of Tumbling Rate

The effect of a variation of the tumbling rate (isotropic rotational diffusion, correlation times between 1 and 0.01 ms) is shown in Fig. 3. It is basically twofold: first, the lineshapes show the expected reduction in linewidth upon an increase of the tumbling rate; second, the transient oscillations are strongly affected in terms of their frequency and the damping behavior. On an increase of the tumbling velocity, the angular contributions to the oscillation frequency start to average out, finally leading to a single line which develops exponentially (Fig. 3e). At the same time, the development of the overall cp signal is slowed down, due to the more efficient motional averaging of the residual dipolar coupling.

Another interesting feature is observed for the zero degree orientation of the axially symmetric tensor (3000 Hz on the frequency axis) at medium tumbling rates: small negative spectral amplitudes are found for 100 μs $< t_{cp} <$ 200 μs. This is caused by a deviation of the initial angular-dependent magnetization after the cp sequence from the equilibrium angular population followed by redistribution due to a more or less efficient motional exchange.

Generally, the changes to single cp spectra and series of spectra under variation of t_{cp} are very dramatic in a dynamic window that is specified by the CSA tensor as well as by the dipolar interaction. Therefore, an analysis of cp lineshapes for dynamic processes generally yields more information than corresponding studies on direct excitation spectra.

Effect of Sample Spinning

The result of a simulated magic angle spinning experiment for two spinning rates (1500 and 2500 Hz) is displayed in Fig. 4. The spectrum for the lower spinning rate (Fig. 4a) exhibits well-dissolved spinning sidebands at ± 1500 Hz with signal

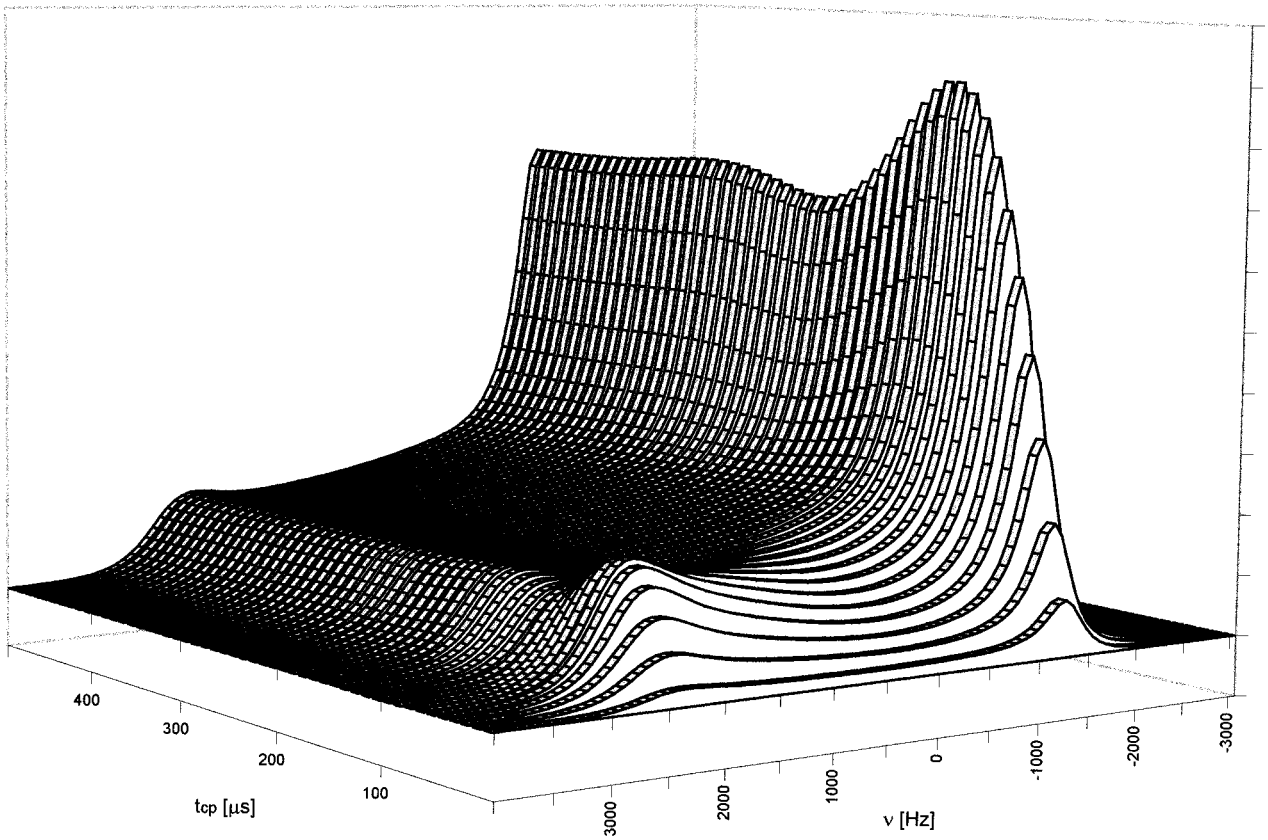

FIG. 6. Stacked plots of calculated cp spectra for various mixing times under the influence of additional I–I dipolar coupling. The relevant time constant T_d is set to 100 μs; all other parameters are identical to those given for Fig. 2.

areas of approximately 0.2 and 0.4 relative to the centerband as expected according to diagrams by Herzfeld and Berger (*17*). The left second spinning sideband at 3000 Hz is barely visible. At the higher spinning rate, the spinning sidebands at $\pm$2500 Hz appear even weaker with average relative intensities of 0.08 and 0.12. The transient oscillations of the MAS signals show a complicated pattern and depend on the sample rotation frequency, as the latter determines the modulation of the dipolar coupling.

A deviation from the magic angle leads to scaled interaction tensors and correspondingly to reduced spectral linewidths under improved signal-to-noise ratios as compared to spectra on static samples. These lineshapes still reflect motional processes and may be analyzed accordingly (*12*, *18*).

Deviation from the Ideal Hartmann–Hahn Condition

Typical changes induced by a given deviation from the Hartmann–Hahn match are represented in Fig. 5. In both cases (a and b), we assume slow isotropic tumbling motion with a correlation time of 1 ms. The simulated mismatch condition (Fig. 5b) is given by a spin lock frequency of 100,000 1/s for I spins and 80,000 1/s for S spins. The resulting changes as compared to a corresponding spectrum for an ideal Hartmann–Hahn match (Fig. 5a) are most significant for the 90° orientation of the symmetric CSA tensor (at $-$1500 Hz spectral frequency). First, the maximum amplitude achieved through cross polarization is reduced by approximately 35% (mainly due to an effective rotation angle φ which here is smaller than 90°); second, the oscillation frequency is slightly increased (due to an increase of the overall rotation frequency ω of the difference vector). The same effects, to a much smaller extent, are detectable for the 0° orientation of the CSA tensor at 3000 Hz spectral frequency. In this case, the larger offset frequency Δ_S partially compensates for the reduced spin lock frequency ω_{1S}. However, the overall changes in lineshape induced by Hartmann–Hahn mismatch are significant; therefore, in a careful analysis, it is crucial to obtain precise knowledge of the matching conditions. Alternatively, one may use ramped amplitude pulses and sweep through the Hartmann–Hahn condition such that all angular positions are equally affected.

Effect of Homonuclear I–I Coupling

In order to demonstrate the effect of the dipolar coupling between the I–S system and abundant I spins, the first model

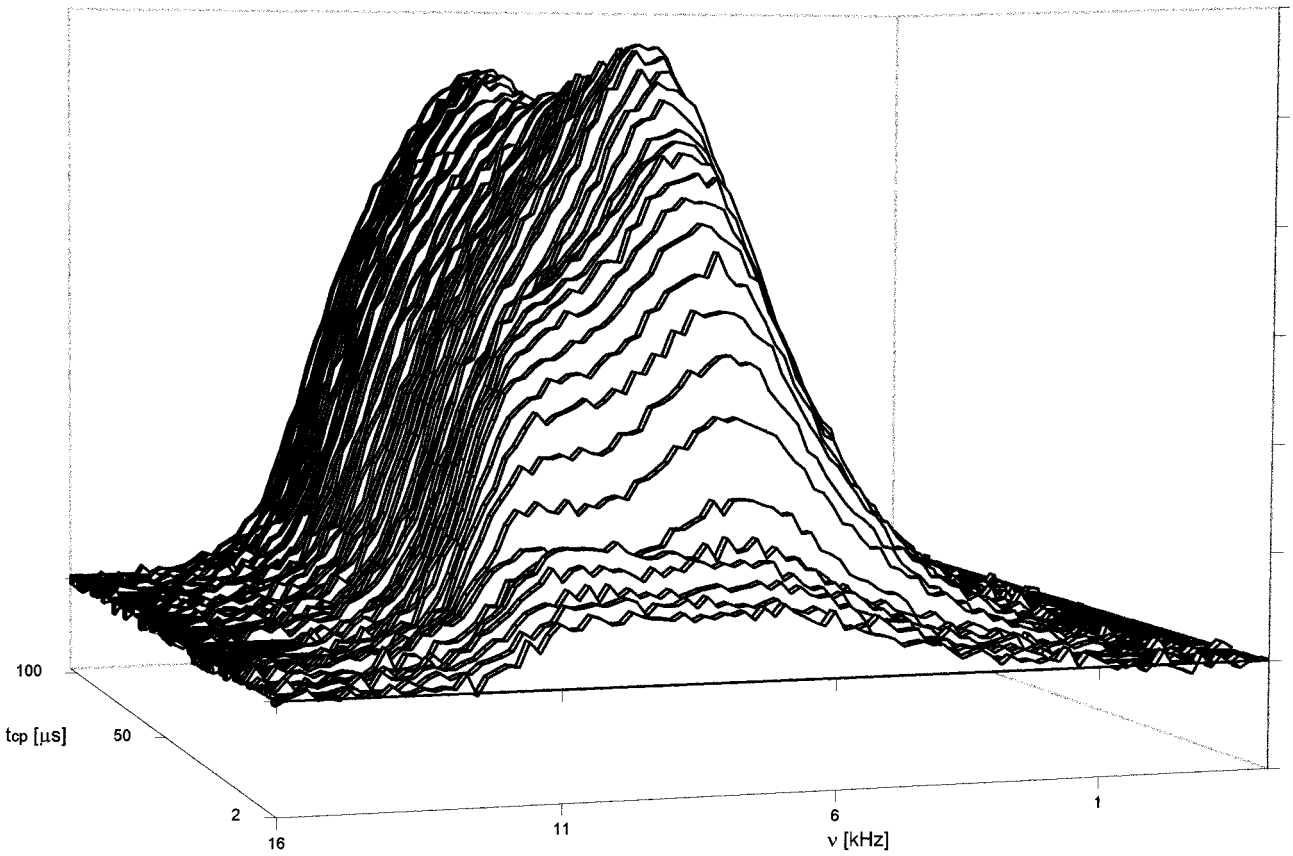

FIG. 7. Experimental cross-polarization carbon spectra of supercooled [2-^{13}C]glycerol at 180 K. The mixing time t_{cp} is varied between 2 and 100 μs in steps of 2 μs. Each spectrum is accumulated from eight scans using a standard cp pulse sequence (see text).

calculation of this series (transient oscillation; see Fig. 2) is reproduced with identical parameters except for the time constant T_d which is set to 100 μs instead of infinity. The resulting spectrum is shown in Fig. 6. As expected, the additional dipolar coupling contributes efficiently to the damping of transient oscillations (compare Fig. 2). In practical applications of the algorithm, the time constant T_d serves as a variable parameter which allows one to fit the experimentally observed oscillation behavior.

REPRESENTATIVE RESULTS

In order to demonstrate the applicability of the simulation procedure, it is used to reproduce an experimental result on a model system. Figure 7 shows a stacked plot of ^{13}C–^{1}H cross-polarization spectra from supercooled [2-^{13}C]glycerol (Cambridge Isotope Laboratories, Andover, MA) taken at 180 K under variation of the cross-polarization mixing time t_{cp} (from 2 to 100 μs in steps of 2 μs). All ^{13}C spectra are obtained at 100.617 MHz resonance frequency by accumulating eight scans using a standard cross-polarization sequence: a $\pi/2$ pulse of 7 μs duration for protons followed by ^{1}H and ^{13}C contact pulses with a duration given by t_{cp}. The spectral lineshapes depend strongly on the length of the mixing period: initially, the spectra exhibit a distinct shoulder in the vicinity of 10 to 12 kHz which decreases and finally disappears for increasing mixing times t_{cp}.

The corresponding best fit simulation based on the assumption of an isotropic rotational diffusion is shown in Fig. 8. The simulation parameters summarized in Table 1 are derived almost independently from typical features of the experimental spectra: the elements of the chemical shift tensor in the principal axis system σ_{XX}, σ_{YY}, σ_{ZZ} may be determined from the low-frequency onset, the position of the central peak of the spectrum, and the high-frequency onset, respectively. The typical features of the spectral lineshapes sensitively reflect the correlation time τ of the rotational diffusion. The frequency and the damping behavior of the transient oscillation allow for the determination of the dipolar coupling parameters D_{IS} and T_d while the orientation of the C–H vector may be derived from the dependence of the cross-polarization rate on the position in the powder spectrum. The initial formation of a distinct shoulder between 10 and 12 kHz indicates that the C–H vector for the central carbon in glycerol points along the x axis of the given principal axis system (see Table 1). With 80 μs, the correlation time for isotropic rotational diffusion of the

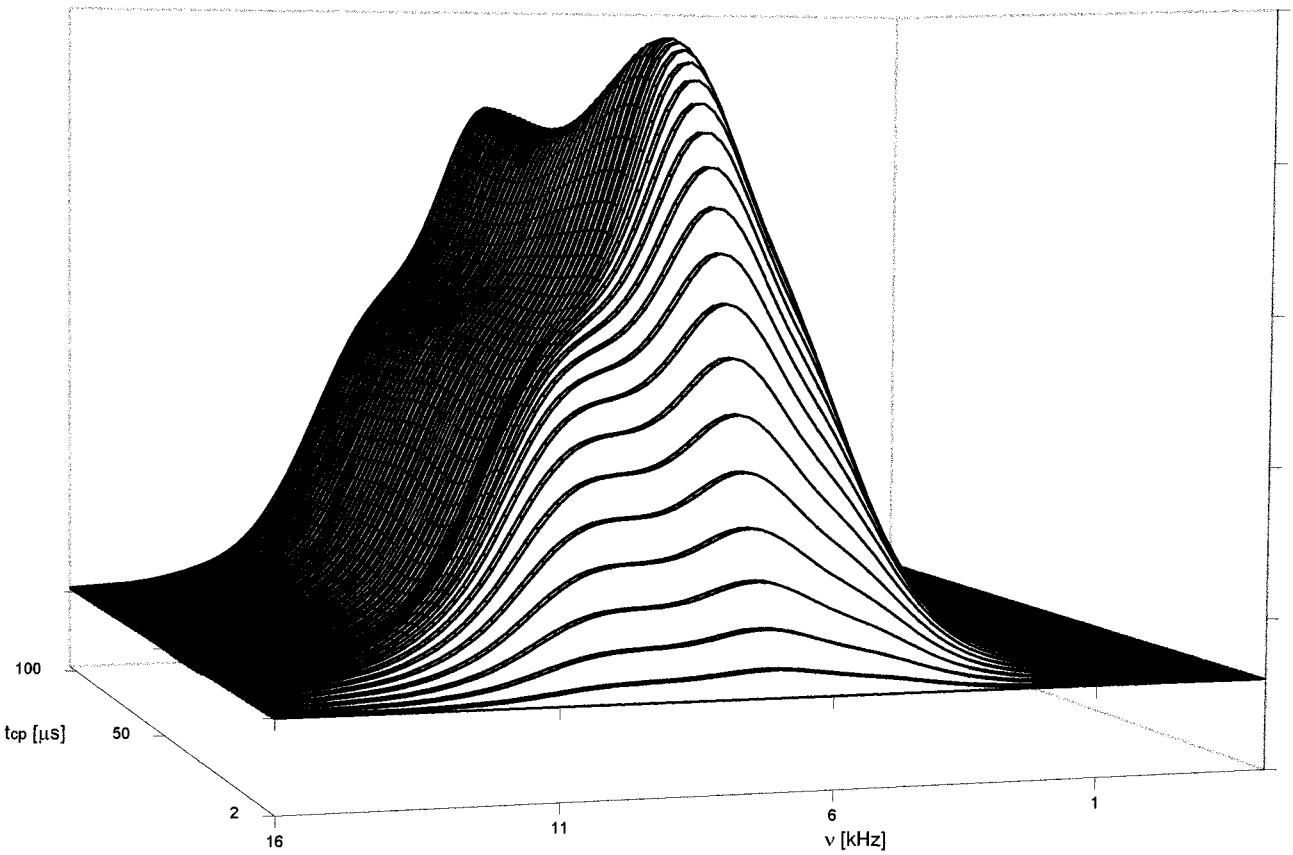

FIG. 8. Calculated best fit for the experimental results shown in Fig. 7. The simulation is based on an isotropic rotational diffusion with a correlation time of 80 μs. The full set of simulation parameters is given in Table 1.

glycerol molecules is within the expected range derived from an extrapolation of data obtained at higher temperatures (*19, 20*).

CONCLUSION

The numeric algorithm described is capable of simulating spectral lineshapes for a large variety of experiments including cp, cp-MAS, cp-(off-angle)-MAS, cp under a given offset from the Hartmann–Hahn condition, and cp using a variable intensity of the contact pulse. Hereby, it allows one to analyze corresponding cp spectra (or series of cp spectra under variation of the contact time) for molecular motions such as rotational diffusion or jump processes. It may also help to find optimal parameter settings for cp experiments on systems with given molecular and structural properties.

TABLE 1

Simulation parameters	Chemical shift tensor (kHz)[a]			Correlation time τ	I–I dipolar damping: T_d	I–S dipolar coupling: D_{IS}	Direction cosines of C–H vector in PAS[b]		
	σ_{XX}	σ_{YY}	σ_{ZZ}						
Best fit data	12.5	7.	3.	80 μs	50 μs	32 kHz $\times (1 - 3\cos^2\theta_{IS})$	x 1	y 0	z 0[c]
Estimated error		±1 kHz		±20%	±20%	±10%		±20%	

[a] Corresponds to 125 ppm/70 ppm/30 ppm.
[b] Principal axes system.
[c] C–H vector points along the x axis of the PAS.

ACKNOWLEDGMENTS

I thank Wiebren S. Veeman for his general support and helpful advice on the issue of cross polarization. With respect to the experimental results, I owe special thanks to Dirk Hoffmann for his valuable practical assistance.

REFERENCES

1. S. R. Hartmann and E. L. Hahn, *Phys. Rev.* **128,** 2024 (1962).
2. A. Pines, M. G. Gibby, and J. S. Waugh, *J. Chem. Phys.* **59,** 569 (1973).
3. M. Matti Maricq and J. S. Waugh, *J. Chem. Phys.* **70,** 3300 (1979).
4. S. Hediger, B. H. Meier, N. D. Kurur, G. Bodenhausen, and R. R. Ernst, *Chem. Phys. Lett.* **223,** 283 (1994).
5. S. Hediger, B. H. Meier, and R. R. Ernst, *Chem. Phys. Lett.* **213,** 627 (1993).
6. D. E. Demco, J. Tegenfeldt, and J. S. Waugh, *Phys. Rev.* **11,** 4133 (1975).
7. F. Engelke, T. Kind, D. Michel, M. Pruski, and B. C. Gerstein, *J. Magn. Reson.* **95,** 286 (1991).
8. D. Marks and S. Vega, *J. Magn. Reson. A* **118,** 157 (1996).
9. D. E. Demco and I. Ardeleanu, *Rom. J. Phys.* **42,** 99 (1997).
10. C. Mayer, *J. Magn. Reson.* **138,** 1 (1999).
11. R. R. Ernst, G. Bodenhausen, and A. Wokaun, "Principles of Nuclear Magnetic Resonance in One and Two Dimensions," Oxford Univ. Press, Oxford (1987).
12. C. Mayer, *J. Magn. Reson.* **139,** 132 (1999).
13. L. Müller, A. Kumar, T. Baumann, and R. R. Ernst, *Phys. Rev. Lett.* **32,** 1402 (1974).
14. A. Abragam, "The Principles of Nuclear Magnetism," Clarendon Press, Oxford (1961).
15. F. Perrin, *J. Phys. Radium* **5,** 497 (1934).
16. F. Perrin, *J. Phys. Radium* **7,** 1 (1936).
17. J. Herzfeld and A. E. Berger, *J. Chem. Phys.* **73,** 6021 (1980).
18. C. Mayer and G. Lukowski, *Pharm. Res.* **17**(4), (2000).
19. M. Wolfe and J. Jonas, *J. Chem. Phys.* **71**(8), 3252 (1979).
20. R. B. Fiorito and R. Meister, *J. Chem. Phys.* **56**(9), 4605 (1972).